Bulletin of Earthquake Engineering
https://doi.org/10.1007/s10518-022-01328-9

ORIGINAL ARTICLE

Effects of magnitude and distance on spectral and pseudospectral acceleration proximities for high damping ratio

Haizhong Zhang[1] · Yan-Gang Zhao[1]

Received: 24 August 2021 / Accepted: 17 January 2022
© The Author(s), under exclusive licence to Springer Nature B.V. 2022

Abstract

The spectral absolute acceleration, *Sa*, is a useful tool for estimating the inertial force that is of interest in foundation design particularly for buildings with energy dissipation or seismic isolation systems. Nevertheless, seismic codes typically specify only the pseudospectral acceleration, *Spa*. Many studies have been performed to clarify the relationship between *Sa* and *Spa* in order to relate the two spectra. A recent study indicated that this relationship could be affected not only by the structural damping ratio and period but also by seismological parameters such as magnitude and distance. However, how these seismological parameters affect their relationship is not clearly understood. To clarify this issue, an approach that relates the two spectra and includes seismological parameters is proposed herein based on random vibration theory. The proposed approach is verified by comparison with the results of time-series analysis. Furthermore, the effects of moment magnitude and source-to-site distance are explored and explained based on the proposed approach. It is found that although *Sa* becomes larger than *Spa* as the structural period and damping ratio increases, this increase becomes smaller with increasing moment magnitude and source-to-site distance due to the increase in the long-period components of earthquake ground motions. Finally, a practical formulation for estimating *Sa* from *Spa* considering the seismological effects is constructed and verified using real seismic records.

Keywords Spectral absolute acceleration · Pseudospectral acceleration · Random vibration theory · Seismological effects · Inertial force

1 Introduction

Response spectrum is presently the most widely used tool for the characterization of seismic loads for seismic designs of buildings. In most seismic codes, particularly those involving force-based design, the response spectrum for the design is typically specified as the 5%-damped pseudospectral acceleration, *Spa*, along with a damping modification

✉ Yan-Gang Zhao
zhao@kanagawa-u.ac.jp

[1] Department of Architecture, Kanagawa University, 3-27-1 Rokkakubashi, Kanagawa-ku, Yokohama 221-8686, Japan

Published online: 15 February 2022

Content courtesy of Springer Nature, terms of use apply. Rights reserved.

factor for adjustment to other damping levels (Akkar et al. 2014; Pu et al. 2016; Zhang and Zhao, 2020). *Spa* is defined based on the spectral relative displacement, *Sd*, according to $Spa = \overline{\omega}^2 Sd$, where $\overline{\omega}$ is the structural circular frequency. Therefore, the force estimated using *Spa* is proportional to the relative displacement, and thus corresponds to the restoring force of the structure. The force estimated using *Spa* can be expressed by $m \cdot Spa = m \cdot \overline{\omega}^2 \cdot Sd = k \cdot Sd$, where m and k are the mass and stiffness of the structure, respectively. Therefore, *Spa* is suitable in the cases where either the restoring force or relative displacement are of interest in the seismic design, e.g., in the design of the superstructures of regular buildings and buildings with energy dissipation devices (Lin and Chang 2003). Nevertheless, the inertial force is of greater interest in the foundation design (Sadek et al. 2000; Mentrasti 2008), because both the restoring force and the damping force, i.e., the inertial force, are transmitted to the foundation, as illustrated by Fig. 1. In the Recommendation for Design of Building Foundations (AIJ 2001) of Japan, the inertial force of structures is considered in the foundation design. Since the force estimated using the spectral absolute acceleration, *Sa*, is proportional to the absolute acceleration and corresponds to the inertial force of the structure, $m \cdot Sa$, *Sa* is more suitable for use in foundation design.

Early studies have shown that for small structural damping ratios, *Sa* can be approximated by *Spa*; however, when the structural damping ratio is large and the structural period is long, *Sa* can differ significantly from *Spa* (Jenschke et al. 1964, 1965; Veletsos and Newmark, 1964; Newmark and Rosenblueth 1971; Boore 2001; Chopra 2007) and is always greater than *Spa* (Newmark and Rosenblueth 1971). The increasingly common structures containing energy dissipation or seismic isolation systems typically exhibit very large damping (Constantinou et al. 1998; Naeim and Kelly 1999). The Docomo Nagano Building located in Japan with viscous damping walls was designed to have an equivalent damping ratio of 20% (Wada et al. 2000). The full-scale experimental results of Chang and Lin (2004) showed that the equivalent damping ratio of a structure with added viscoelastic dampers can be larger than 26%. Furthermore, the experimental results of Wolff et al. (2014) indicated that the equivalent damping ratio of seismically isolated structures can be as large as 67% depending on the damping devices used. Therefore, in the foundation design for buildings with energy dissipation or seismic

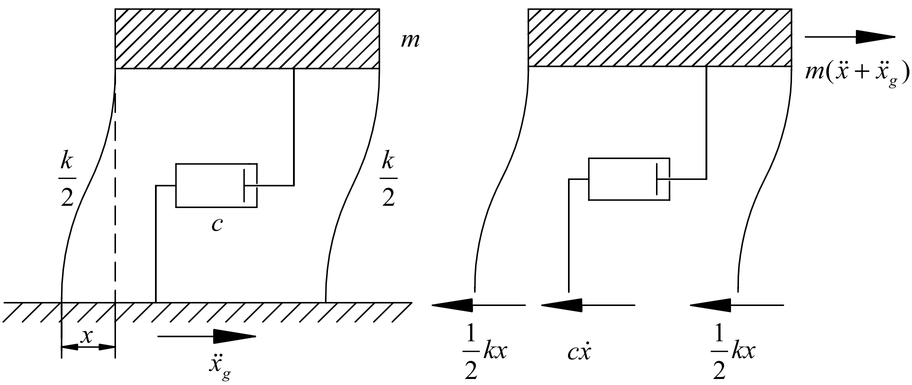

Fig. 1 Illustration of the restoring force (kx), the damping force ($c\,\dot{x}$), and the inertial force ($m(\ddot{x}+\ddot{x}_g)$) considering a single-degree-of-freedom structure, where, x is the relative displacement, x_g is input earthquake acceleration, and c is the damping coefficient

Content courtesy of Springer Nature, terms of use apply. Rights reserved.

isolation systems, the direct use of *Spa* to approximate *Sa* may underestimate the inertial forces and negatively affect the design.

Development of an additional *Sa* for seismic design is an alternative approach for solving the problem described above. However, this approach requires the repetition of the procedure for defining *Spa* in seismic codes, namely (1) the derivation of a ground-motion prediction equation for 5%-damped *Sa*, (2) execution of a probabilistic seismic hazard assessment to obtain *Sa* for the target hazard levels (Alamilla et al. 2020), and (3) development of an equation for the damping modification factor to adjust the 5%-damped *Sa* to other damping levels. To avoid repeating this complicated procedure, many studies have been conducted to elucidate the relationship between *Sa* and *Spa* in order to relate them directly. Sadek et al. (2000) compared these two spectra based on statistical analyses of 72 accelerograms from 36 stations in the western United States. Song et al. (2007) derived an analytical equation to relate these two spectra by assuming that the earthquake excitation is a Gaussian stationary process. Mentrasti (2008) theoretically analyzed and explained the relationship between these two spectra based on exact integral analysis. Zhang et al. (2016) discussed these spectra and compared them based on the El Centro earthquake record.

The above studies have yielded useful results on the relationship between the two spectra as well as the effects of the structural parameters, namely the structural period and the damping ratio. Papagiannopoulos et al. (2013) further noted that the relationship between them is affected not only by the structural but also by seismological parameters, e.g., magnitude and distance, based on the statistical analyses of 866 accelerograms recorded worldwide. However, the principle underlying how the seismological parameters affect the relationship between the two spectra has not been elucidated.

This paper aims to clarify the effects of magnitude and distance on the relationship between *Sa* and *Spa*. The remainder of this paper is organized as follows. First, an approach to relate *Sa* and *Spa* that includes seismological parameters is developed based on the random vibration theory (RVT). This approach is then verified by comparison with the results of time-series analysis. Subsequently, based on the developed approach, the effects of moment magnitude and source-to-site distance on the relationship between the two spectra are systematically investigated and theoretically explained. Furthermore, a practical formulation for estimating *Sa* from *Spa* considering the seismological effects is constructed and verified using real seismic records. Finally, the conclusions of this study are stated.

2 Approach to relate *Sa* and *Spa*

To investigate the effects of magnitude and distance on the relationship between *Sa* and *Spa*, the following two approaches may be feasible: using real accelerograms or ground-motion prediction equations for *Sa* and *Spa*. However, to identify consistent patterns within an appreciable margin of variability that is always displayed by strong-motion data, large numbers of records must be employed because one is unlikely to find records that are essentially similar in all but one characteristic. In addition, although there are many available ground-motion prediction equations for the 5%-damped *Spa* (Douglas 2021), very few such equations are available for 5%-damped compatible *Sa* and *Spa* and even fewer are available for compatible *Sa* and *Spa* with various damping ratios. Therefore, based on the ability of the RVT to relate the FAS to the response spectrum, this study adopts a Fourier amplitude spectrum (FAS) ground-motion model and RVT to estimate and relate the

Content courtesy of Springer Nature, terms of use apply. Rights reserved.

two spectra. The proposed analytical approach allows the investigation of the seismological effects as well as a theoretical explanation for the observed phenomena.

2.1 Earthquake ground-motion model

Various methods are available in the literature to describe the FAS of the earthquake ground motions. The simplest method involves using seismology theory to compute the radiated FAS from a point source in terms of the various source, path, and site parameters. This study utilizes the seismological point-source theory to derive the FAS based on the description by Boore (2003). The FAS of the ground-motion acceleration, $Y(f)$ (cm/s), can be expressed as

$$Y(f) = \left[0.78\frac{\pi}{\rho\beta^3}M_0\frac{f^2}{1 + (f/f_c)^2}\right]\left[Z(R)\times\exp\left(\frac{-\pi fR}{Q(f)\beta}\right)\right]\left[\exp(-\pi\kappa_0 f)A(f)\right] \quad (1)$$

where f is the frequency (Hz); ρ is the mass density of the crust (g/cm^3); β is the shear-wave velocity of the crust (km/s); R is the distance from the source (km); $Z(R)$ is the geometric attenuation; κ_0 is the site diminution (s); $Q(f)$ is the anelastic attenuation; $A(f)$ is the crust amplification; M_0 is the seismic moment (dyne cm), which is related to the moment magnitude, M, as $M_0 = 10^{1.5M+10.7}$; f_c is the corner frequency given as $f_c = 4.9\times10^6\beta(\Delta\sigma/M_0)^{1/3}$; and $\Delta\sigma$ is the stress drop (bars). This FAS model has been thoroughly investigated and verified using real seismic records (Atkinson and Boore 2014; Boore 2003), and has been extensively used by numerous studies (Rathje and Ozbey 2006; Kottke and Rathje 2013; Wang and Rathje 2016). The values of the seismological parameters required in Eq. (1) for central and eastern North America (CENA) are used in this study and are determined according to Boore and Thompson (2015). The parameters are taken from the study of Wang and Rathje (2016) and are listed in Table 1.

2.2 Expression for *Sa*/*Spa*

Based on the RVT, both *Sa* and *Spa* can be obtained from the FAS. The RVT states that the peak value of a time-series signal is equal to the product of the peak factor and root-mean-square (rms) value, which can be expressed as

Table 1 Parameters used to develop FAS and time series of the rock motion

Parameter	Value
Source spectrum	Brune ω-squared point source
Stress drop $\Delta\sigma$ (bar)	400
Site diminution κ_0 (s)	0.006
Density of crust ρ (g/cm^3)	2.8
Shear-wave velocity of crust β (km/s)	3.7
Geometrical spreading	Atkinson and Boore (2014)
Path attenuation	Atkinson and Boore (2014)
Crustal amplification	Boore (2015)
Duration model	Boore and Thompson (2015)

Content courtesy of Springer Nature, terms of use apply. Rights reserved.

$$a_{max} = pf\sqrt{\frac{1}{D\pi}\int_0^\infty |y(\omega)|^2 d\omega} \tag{2}$$

where $a_{\max}$ is the peak value of the signal, pf denotes the peak factor, the square-root part in Eq. (2) represents the rms value of the signal, which is obtained from the signal duration D and FAS of the signal $y(\omega)$, and ω is the circular frequency ($\omega = 2\pi f$). Since the response spectrum is the peak response value of a single-degree-of-freedom (SDOF) oscillator, according to RVT, the response spectrum should be equal to the product of the peak factor and the rms of the oscillator response. Boore (2003) derived an expression for *Spa* as

$$Spa(\overline{\omega}, \xi) = pf_{p\xi}\sqrt{\frac{1}{D_{\mathrm{rms}}\pi}\int_0^\infty \left|Y_R(\omega, \overline{\omega}, \xi)\right|^2 d\omega} \tag{3}$$

where, $\overline{\omega}$ and ξ are the SDOF-oscillator circular frequency and damping ratio, respectively; $pf_{p\xi}$ is the peak factor of the oscillator response, and the square-root part in Eq. (3) represents the rms value of the oscillator response, that is obtained using the rms duration of the oscillator, D_{rms}, and oscillator-response FAS, $Y_R(\omega, \overline{\omega}, \xi)$. Here, $Y_R(\omega, \overline{\omega}, \xi)$ is equal to the product of the ground-motion FAS $Y(\omega)$ and modulus of the oscillator transfer function for *Spa*, $H_{pa}(\omega, \overline{\omega}, \xi)$, i.e., $Y_R(\omega, \overline{\omega}, \xi) = Y(\omega)\left|H_{pa}(\omega, \overline{\omega}, \xi)\right|$. $H_{pa}(\omega, \overline{\omega}, \xi)$ is expressed as

$$\left|H_{pa}(\omega, \overline{\omega}, \xi)\right| = \frac{1}{\sqrt{(2\xi\omega/\overline{\omega})^2 + ((\omega/\overline{\omega})^2 - 1)^2}} \tag{4}$$

The oscillator transfer function for *Spa*, $H_{pa}(\omega, \overline{\omega}, \xi)$, is obtained from that for *Sd*, $H_d(\omega, \overline{\omega}, \xi)$, through multiplication by $\overline{\omega}^2$, i.e., $\left|H_{pa}(\omega, \overline{\omega}, \xi)\right| = \overline{\omega}^2\left|H_d(\omega, \overline{\omega}, \xi)\right|$. $H_d(\omega, \overline{\omega}, \xi)$ is expressed as

$$\left|H_d(\omega, \overline{\omega}, \xi)\right| = \frac{1/\overline{\omega}^2}{\sqrt{(2\xi\omega/\overline{\omega})^2 + ((\omega/\overline{\omega})^2 - 1)^2}} \tag{5}$$

In the RVT analysis, the direct transformation of *Sd* to *Spa* by $Spa = \overline{\omega}^2 \times Sd$ is equivalent to the above approach of transforming the oscillator transfer function by $\left|H_{pa}(\omega, \overline{\omega}, \xi)\right| = \overline{\omega}^2\left|H_d(\omega, \overline{\omega}, \xi)\right|$. This is attributed to the property of Eq. (3) in which the integral of $Y_R(\omega, \overline{\omega}, \xi)$ is related to ω; thus, one can insert $\overline{\omega}^2$ into the integral, i.e., transform $H_d(\omega, \overline{\omega}, \xi)$, or put it outside the radical sign, i.e., transform *Sd*, to obtain the same results.

Similarly, based on the RVT, *Sa* can be obtained by replacing the oscillator transfer function, the rms duration, and the oscillator-response peak factor for *Spa* in Eq. (3) by those for *Sa*. The oscillator transfer function for *Sa*, $H_a(\omega, \overline{\omega}, \xi)$, is given by (Ohsaki 1996)

$$\left|H_a(\omega, \overline{\omega}, \xi)\right| = \frac{\sqrt{(2\xi\omega/\overline{\omega})^2 + 1}}{\sqrt{(2\xi\omega/\overline{\omega})^2 + ((\omega/\overline{\omega})^2 - 1)^2}} \tag{6}$$

Then, the expression for the ratio of *Sa* to *Spa* can be obtained using the respective spectra:

Content courtesy of Springer Nature, terms of use apply. Rights reserved.

$$\frac{Sa(\overline{\omega},\xi)}{Spa(\overline{\omega},\xi)}=\sqrt{\frac{\int_0^\infty \left|Y(\omega)H_a(\omega,\overline{\omega},\xi)\right|^2 d\omega}{\int_0^\infty \left|Y(\omega)H_{pa}(\omega,\overline{\omega},\xi)\right|^2 d\omega}}\times\frac{pf_\xi}{pf_{p\xi}}\sqrt{\frac{D_{\mathrm{rms}}}{Da_{\mathrm{rms}}}} \tag{7}$$

where, pf_ξ and Da_{rms} are the oscillator-response peak factor and the rms duration for *Sa*, respectively. Thus, Eq. (7) theoretically relates the two spectra.

To apply Eq. (7) to estimate *Sa*/*Spa*, the rms durations for *Spa* and *Sa*, i.e., D_{rms} and Da_{rms}, must be determined. While three models for D_{rms} have been developed (Boore and Joyner 1984; Boore and Thompson 2012, 2015; Liu and Pezeshk 1999), no investigations related to Da_{rms} have been reported. In addition, although the D_{rms} models include the damping ratio ξ, only *Spa* for 5% damping ratio have been verified. To enable the implementation of Eq. (7) to explore *Sa*/*Spa*, the rms duration for *Sa* is assumed to be the same as that for *Spa*, i.e., $Da_{\mathrm{rms}}=D_{\mathrm{rms}}$, so that the duration term ($\sqrt{D_{\mathrm{rms}}/Da_{\mathrm{rms}}}$) in Eq. (7) disappears. In fact, errors caused by this assumption are very limited, as described in detail in the next section. Therefore, the expression for *Sa*/*Spa* in Eq. (7) can be decomposed into two terms: the first term (i.e.,$\sqrt{\int_0^\infty \left|Y(\omega)H_a(\omega,\bar{\omega},\xi)\right|^2 d\omega}/\sqrt{\int_0^\infty \left|Y(\omega)H_{pa}(\omega,\bar{\omega},\xi)\right|^2 d\omega}$) is the ratio of the oscillator-response rms values for *Sa* and *Spa*, hereafter denoted as R_{rms}; and the second term (i.e., $pf_\xi/pf_{p\xi}$) is the ratio of the oscillator-response peak factors for *Sa* and *Spa*, hereafter denoted as R_{pf}.

To apply Eq. (7) to estimate the ratio of the two spectra, the value of the peak factor also must be determined. Many models have been developed for the estimation of the peak factor (Cartwright and Longuet-Higgins 1956; Davenport 1964; Vanmarcke 1975). Among these, the model by Vanmarcke (1975) has been found to provide the most reasonable estimations of the response spectra in RVT analysis (Boore and Thompson 2015; Wang and Rathje 2016). The cumulative distribution function, *P*, of the peak factor, *pf*, as provided by Vanmarcke (1975) is given by

$$P(pf<r)=[1-e^{(-r^2/2)}]\times\exp[-2f_z\exp(-r^2/2)D_{gm}\frac{(1-e^{-\delta^{1.2}r\sqrt{\pi/2}})}{(1-e^{r^2/2})}] \tag{8}$$

Here, δ is a bandwidth factor that is defined as a function of the spectral moments:

$$\delta=\sqrt{1-\frac{m_1^2}{m_0m_2}} \tag{9}$$

where m_0, m_1, and m_2 denote the zeroth-, first-, and second-order moments of the square of the FAS, and the *n*th-order spectral moment, m_n, of a FAS $y(\omega)$ is defined as

$$m_n=\frac{1}{\pi}\int_0^\infty \omega^n|y(\omega)|^2d\omega \tag{10}$$

In Eq. (10), when one calculates the peak factor of the ground motion, the ground-motion FAS should be used, while when one calculates the oscillator-response peak factors, i.e., $pf_{p\xi}$ and pf_ξ, the oscillator-response FAS should be used accordingly. In addition, f_z denotes the rate of zero crossings that is also a function of the spectral moments, and is given by

Content courtesy of Springer Nature, terms of use apply. Rights reserved.

$$f_z = \frac{1}{2\pi}\sqrt{\frac{m_2}{m_0}} \tag{11}$$

Boore and Joyner (1984) found that good results can be obtained if the ground-motion duration D_{gm} is used for the estimation of the peak factor, and the rms duration D_{rms} is used for the estimation of the rms value of the oscillator response. Therefore, the ground-motion duration D_{gm} is used in Eq. (8) to estimate $pf_{p\xi}$ and pf_{ξ}. In addition, D_{gm} is determined based on the model of Boore and Thompson (2014, 2015). In RVT analysis, the expected value of the peak factor is always used and can be obtained using Eq. (8) by the expression $\int_0^{\infty}[1-P(pf<r)]dr$.

3 Verification

To investigate the accuracy of the proposed approach, the ratio of the two spectra, *Sa*/*Spa*, was calculated using Eq. (7) and compared to that obtained using traditional time-series analysis. The time series for the analysis was generated from ground-motion FAS using the SMSIM (Boore 2005) program via stochastic simulations (Boore 1983). For each FAS, a suite of 100 time-series signals was generated, and the simulated time series matched the FAS on average. Then, the values of *Sa*, *Spa*, and the spectral ratios *Sa*/*Spa* for all of the generated time series were calculated using the direct integration method of Nigam and Jennings (1969). For each FAS, the 100 corresponding results of the spectral ratios *Sa*/*Spa* for a given damping level were averaged and compared to those obtained using the proposed approach. A wide range of the structural parameters, i.e., oscillator period T_0 (0.01–10 s) and damping ratio ξ (10–50%), as well as main seismological parameters, including the moment magnitude M (4–8) and site-to-source distance R (20–200.01 km), were considered in the calculations. Some of these representative comparisons are shown in Figs. 2, 3, 4. It is found that the results obtained by the proposed approach are in good agreement with the results obtained by the time-series analysis. The maximum relative error is limited to approximately 10%, and the average relative error for all of the considered cases is approximately 5%. The good agreement between the proposed approach and the time-series analysis not only validates the proposed approach but also supports the rationality of the assumption that $Da_{\text{rms}} = D_{\text{rms}}$, in Sect. 2.2.

The figures also clearly show the relationship between the two spectra. It is observed that the values of *Sa*/*Spa* are greater than unity for all cases, implying that *Sa* is always greater than *Spa*. Figure 2 also indicates that *Sa*/*Spa* is nearly equal to unity at small oscillator periods and increases with increasing oscillator periods and damping ratios; these values may be considerably greater than unity for very long oscillator periods and very large damping ratios. These observed properties for the relationship between the two spectra are consistent with those observed by statistical analyses of real seismic records (Jenschke et al. 1964, 1965; Veletsos and Newmark 1964; Newmark and Rosenblueth 1971; Sadek et al. 2000; Boore 2001; Chopra 2007; Song et al. 2007; Mentrasti 2008; Papagiannopoulos et al. 2013; Zhang et al. 2016). The consistency of these observations provides additional confirmation of the proposed approach.

Content courtesy of Springer Nature, terms of use apply. Rights reserved.

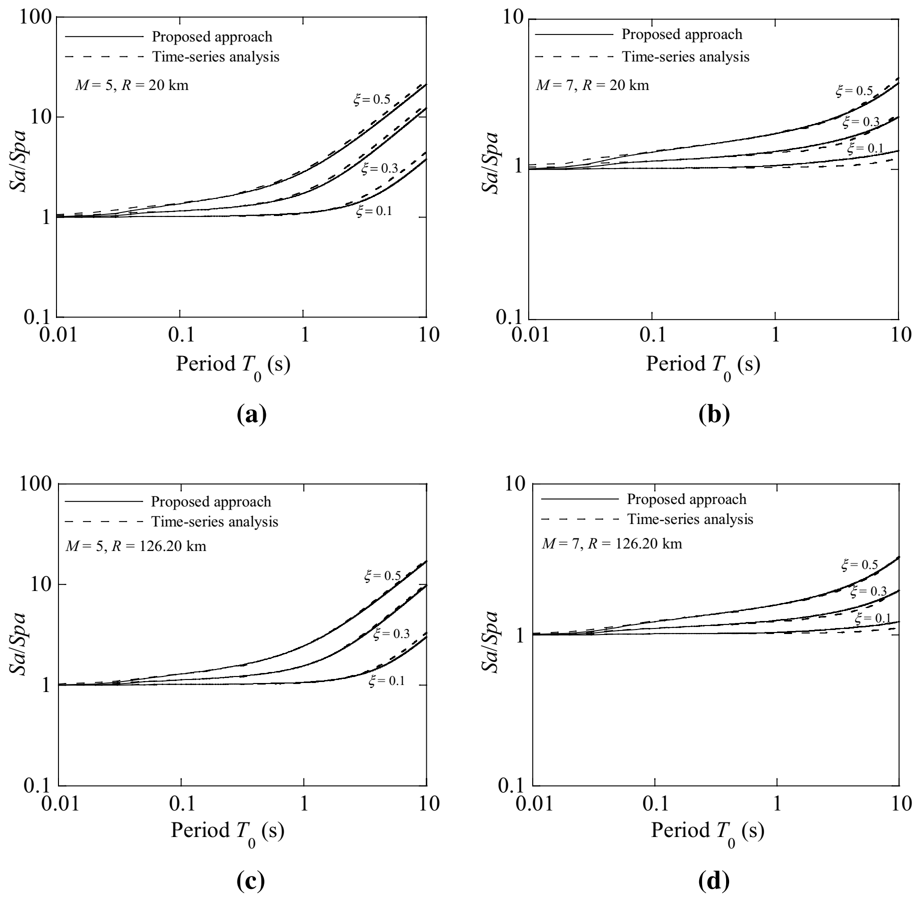

Fig. 2 Variation of spectral ratio *Sa*/*Spa* with oscillator damping ratio ξ for cases with moment magnitude M and site-to-source distance R of (**a**) $M=5$, $R=20$ km, (**b**) $M=7$, $R=20$ km, (**c**) $M=5$, $R=126.20$ km, and (**d**) $M=7$, $R=126.20$ km

4 Effects of magnitude and distance on the *Sa*-*Spa* relationship

4.1 Exploration of effects of magnitude and distance

This section investigates the effects of moment magnitude and site-to-source distance on the relationship between *Sa* and *Spa* based on the proposed approach. From Figs. 3 and 4 in the previous section, the *Sa*/*Spa* trends for variation of the moment magnitude and site-to-source distance can be easily clarified. Figure 3 indicates that *Sa*/*Spa* is strongly affected by the moment magnitude. The values of *Sa*/*Spa* at long oscillator periods decrease with increasing moment magnitude. This means that although *Sa* becomes larger than *Spa* as the structural period and damping ratio increase, this increase becomes smaller with increasing moment magnitude. Figure 4 indicates that the behavior of *Sa*/*Spa* with variation of the site-to-source distance R is typically consistent with the variation of the moment magnitude albeit with a much smaller degree of variation.

Content courtesy of Springer Nature, terms of use apply. Rights reserved.

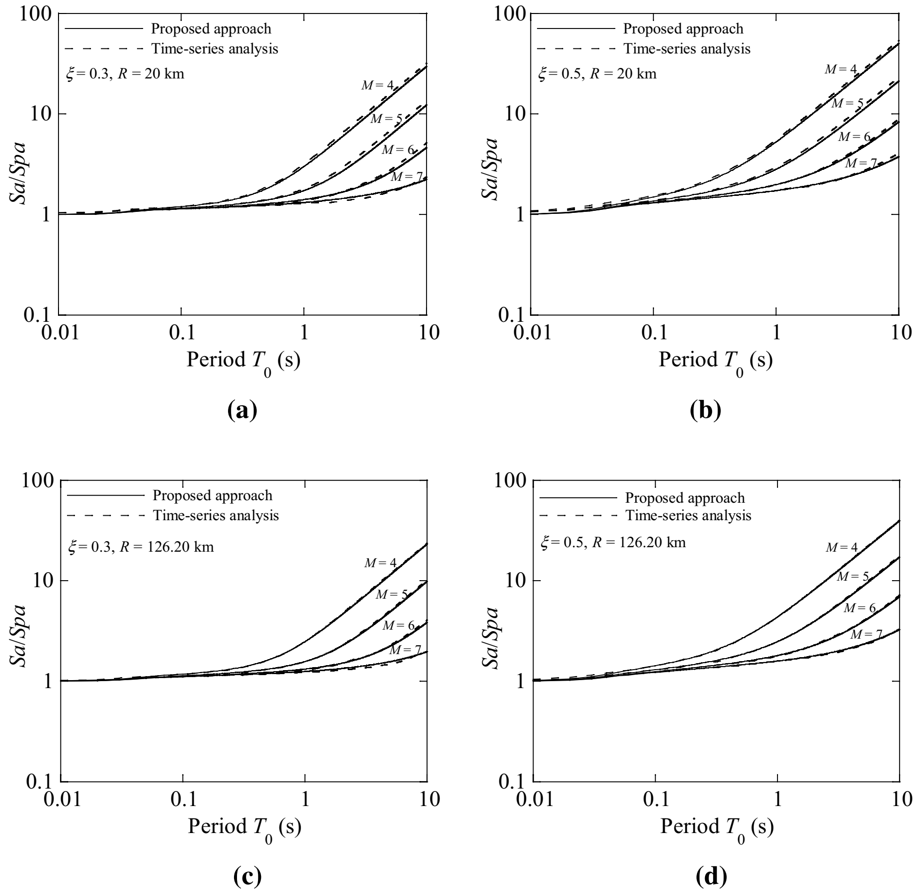

Fig. 3 Variation of spectral ratio *Sa*/*Spa* with moment magnitude *M* for cases with oscillator damping ratio ξ and site-to-source distance *R* of (**a**) $\xi = 0.3$, $R = 20$ km, (**b**) $\xi = 0.5$, $R = 20$ km, (**c**) $\xi = 0.3$, $R = 126.20$ km, and (**d**) $\xi = 0.5$, $R = 126.20$ km

4.2 Explanation of the observed phenomenon

The observed phenomena can be theoretically explained based on the proposed approach. The representative results of the two terms in Eq. (7), i.e., R_{rms} and R_{pf}, for the cases in Fig. 3 are shown in Figs. 5 and 6 to investigate their contributions to *Sa*/*Spa*. It is evident from Figs. 3 and 5 that the value of *Sa*/*Spa* is similar to that of R_{rms}, and all of the characteristics of the *Sa*/*Spa* values, including the trends with variations in the structural and seismological parameters, are captured adequately by R_{rms}. In addition, Fig. 6 indicates that the value of R_{pf} is close to unity. These observations indicate that *Sa*/*Spa* is dominated by R_{rms}, which facilitates explanation of the phenomenon based on R_{rms}. In addition, the similarity between the *Sa*/*Spa* values obtained by the time-series analysis and the R_{rms} values also implies that contribution of the duration term in Eq. (7) ($\sqrt{D_{\mathrm{rms}}/Da_{\mathrm{rms}}}$) to *Sa*/*Spa* is limited, providing further support for the validity of the assumption that $Da_{\mathrm{rms}} = D_{\mathrm{rms}}$, in Sect. 2.2.

Content courtesy of Springer Nature, terms of use apply. Rights reserved.

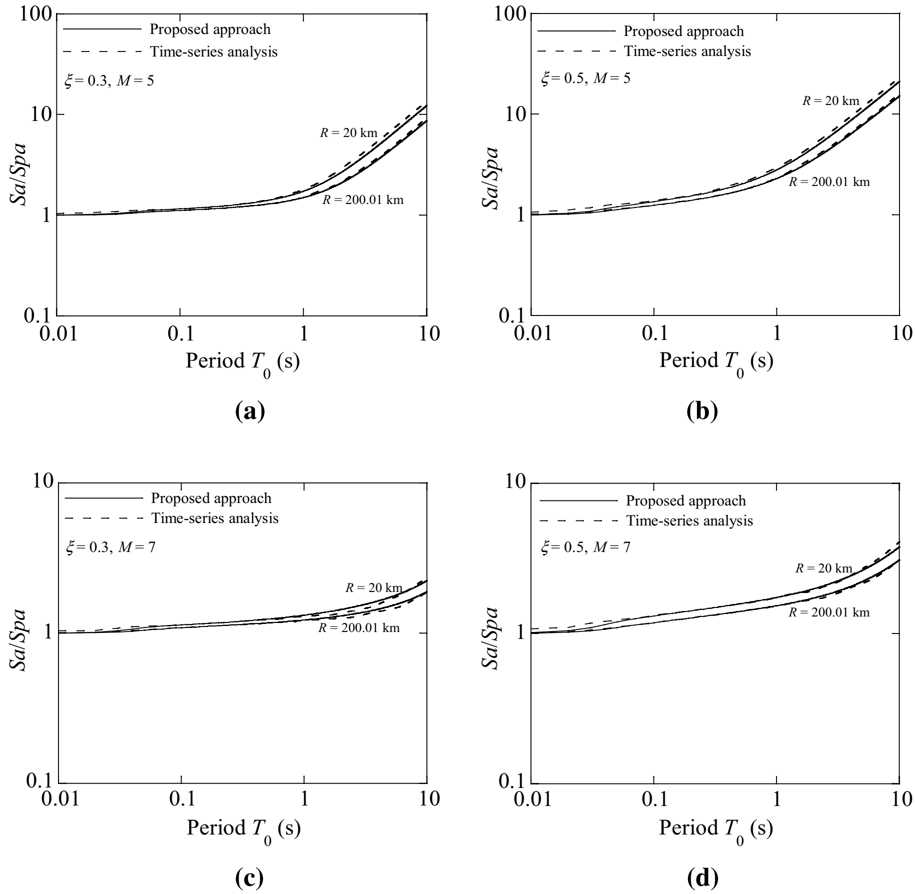

Fig. 4 Variation of spectral ratio *Sa*/*Spa* with site-to-source distance *R* for cases with oscillator damping ratio ξ and moment magnitude *M* of (**a**) $\xi=0.3$, $M=5$, (**b**) $\xi=0.5$, $M=5$, (**c**) $\xi=0.3$, $M=7$, and (**d**) $\xi=0.5$, $M=7$

To facilitate further analysis, the integral terms in the numerator and denominator of $R_{\rm rms}$, i.e., $\int_0^\infty \left|Y(\omega)H_a(\omega,\overline{\omega},\xi)\right|^2 d\omega$ and $\int_0^\infty \left|Y(\omega)H_{pa}(\omega,\overline{\omega},\xi)\right|^2 d\omega$, are regarded as the areas of the square of the oscillator-response FAS enclosed by the circular frequency axis. The integral term in the numerator, i.e., $\int_0^\infty \left|Y(\omega)H_a(\omega,\overline{\omega},\xi)\right|^2 d\omega$, corresponds to *Sa* and that in the denominator, i.e., $\int_0^\infty \left|Y(\omega)H_{pa}(\omega,\overline{\omega},\xi)\right|^2 d\omega$, corresponds to *Spa*. Thus, the proximity between the two spectra or the value of *Sa*/*Spa* is determined by the proximity between these two areas. The closer the two areas are, the more similar are the two spectra, and the closer is the value of *Sa*/*Spa* to unity. It can be further observed from $R_{\rm rms}$ that the ground-motion FAS $Y(\omega)$ in the two integral terms is the same, but the oscillator transfer functions, i.e., $H_a(\omega,\overline{\omega},\xi)$ and $H_{pa}(\omega,\overline{\omega},\xi)$, are different, which can cause the difference between the two areas.

Content courtesy of Springer Nature, terms of use apply. Rights reserved.

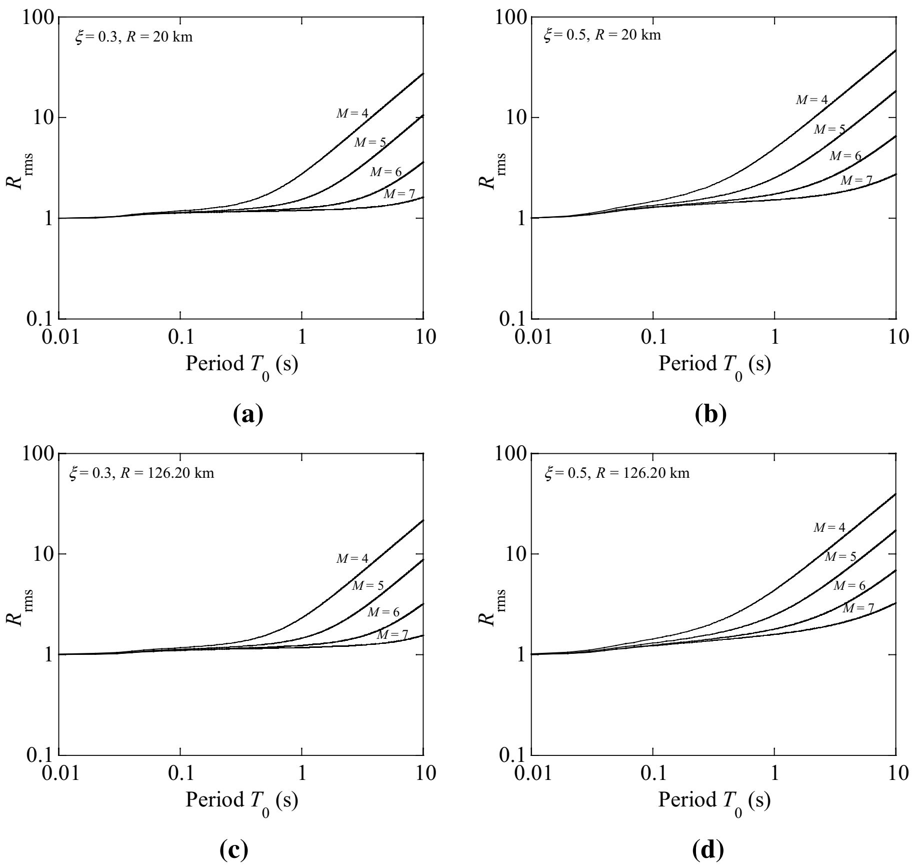

Fig. 5 Variation of the first term of Eq. (7) with moment magnitude M for cases with oscillator damping ratio ξ and site-to-source distance R of (**a**) $\xi=0.3$, $R=20$ km, (**b**) $\xi=0.5$, $R=20$ km, (**c**) $\xi=0.3$, $R=126.20$ km, and (**d**) $\xi=0.5$, $R=126.20$ km

To investigate the differences between the oscillator transfer functions for *Sa* and *Spa*, their values for two oscillator damping ratios, namely 5% and 30%, are compared in Fig. 7. The oscillator frequency f_0 ($f_0=1/T_0$) was chosen as 2 Hz. Here, it should be noted that the oscillator frequency f_0 is different from the frequency f of the ground-motion FAS. It can be found that the two oscillator transfer functions are very similar for the smaller oscillator damping ratio (5%). However, with the increase in the oscillator damping ratio, the difference between the two oscillator transfer functions increases in the high-frequency region. Nevertheless, at the frequencies lower than the oscillator frequency f_0, the values of the two oscillator transfer functions are still quite similar. In addition, it should be noted that values of $H_a(\omega, \overline{\omega}, \xi)$ are always greater than those of $H_{pa}(\omega, \overline{\omega}, \xi)$, and the degree increases with increasing oscillator damping ratios at high frequencies. Based on these properties of the oscillator transfer functions, the *Sa*/*Spa* trends with variations in the oscillator damping ratio can be clarified. Because the difference between the two oscillator transfer functions increases with increasing oscillator damping ratio, the difference between the two integral areas, i.e., $\int_0^\infty \left|Y(\omega)H_a(\omega, \overline{\omega}, \xi)\right|^2 d\omega$

Content courtesy of Springer Nature, terms of use apply. Rights reserved.

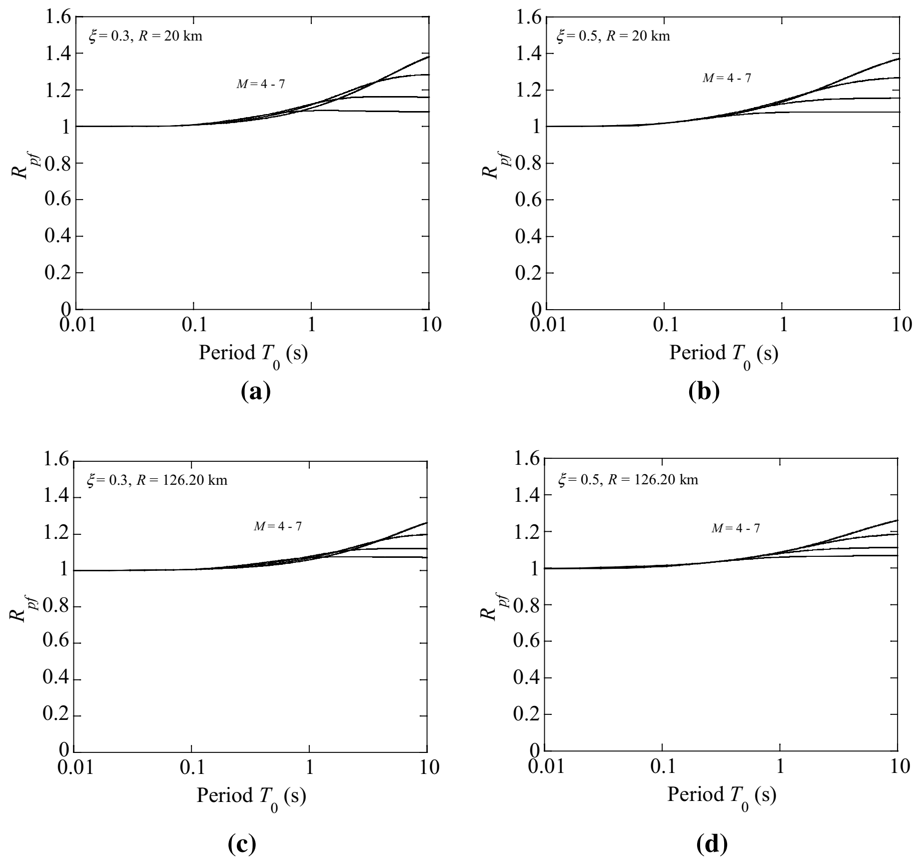

Fig. 6 Variation of the second term of Eq. (7) with moment magnitude M for cases with oscillator damping ratio ξ and site-to-source distance R of (**a**) $\xi=0.3$, $R=20$ km, (**b**) $\xi=0.5$, $R=20$ km, (**c**) $\xi=0.3$, $R=126.20$ km, and (**d**) $\xi=0.5$, $R=126.20$ km

Fig. 7 Comparison of oscillator transfer functions for spectral and pseudospectral accelerations for two oscillator damping ratios (5% and 30%)

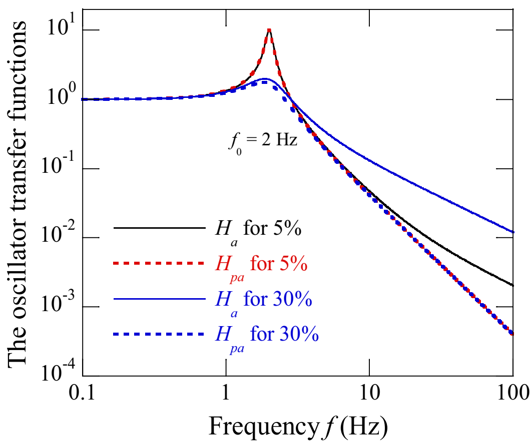

Content courtesy of Springer Nature, terms of use apply. Rights reserved.

and $\int_0^\infty \left|Y(\omega)H_{pa}(\omega,\overline{\omega},\xi)\right|^2 d\omega$, will increase. This causes an increase in the difference between the two spectra with increasing oscillator damping ratios (Fig. 2). Furthermore, because the value of the oscillator transfer function for *Sa* is always greater than that for *Spa*, $\int_0^\infty \left|Y(\omega)H_a(\omega,\overline{\omega},\xi)\right|^2 d\omega > \int_0^\infty \left|Y(\omega)H_{pa}(\omega,\overline{\omega},\xi)\right|^2 d\omega$ and the value of *Sa* is always larger than that of *Spa,* as shown in Figs. 2, 3, 4.

To explain the *Sa*/*Spa* trend with variation in the oscillator period, square values of the two oscillator transfer functions for two different oscillator frequencies (1 and 10 Hz) are compared in Fig. 8. The oscillator damping ratio is set to 30% for comparison. It is observed that due to the decrease in the oscillator frequency f_0, the region of the oscillator transfer functions with frequencies higher than the oscillator frequency f_0 (i.e., $f>f_0$) increases. Because the values of these two transfer functions are quite different in this region, the values of $\left|Y(\omega)H_a(\omega,\overline{\omega},\xi)\right|^2$ and $\left|Y(\omega)H_{pa}(\omega,\overline{\omega},\xi)\right|^2$ are also different in this region, as shown in Fig. 9. Therefore, the region where $\left|Y(\omega)H_a(\omega,\overline{\omega},\xi)\right|^2$ differs from $\left|Y(\omega)H_{pa}(\omega,\overline{\omega},\xi)\right|^2$ increases with decreasing oscillator frequencies. This means that the difference between the two areas given by the numerator $\int_0^\infty \left|Y(\omega)H_a(\omega,\overline{\omega},\xi)\right|^2 d\omega$ and denominator $\int_0^\infty \left|Y(\omega)H_{pa}(\omega,\overline{\omega},\xi)\right|^2 d\omega$ of $R_{\rm rms}$ increases with decreasing oscillator frequencies. This explains the increase in the differences between the two spectra or in the values of *Sa*/*Spa* with decreasing oscillator frequencies (i.e., increasing oscillator periods), as shown in Figs. 2, 3, 4.

To explain the *Sa*/*Spa* trend with variations in the seismological parameters, namely the moment magnitude and site-to-source distance, the key factor governing the seismological effects is investigated in accordance with $R_{\rm rms}$ in Eq. (7). It is observed that the seismological parameters affect $R_{\rm rms}$ by changing the ground-motion FAS. The other components affecting the oscillator-response FAS in $R_{\rm rms}$, i.e., the oscillator transfer functions, are independent of the seismological parameters. Moreover, it is known that the distribution of the ground-motion FAS with frequency instead of absolute values of the FAS affects the first

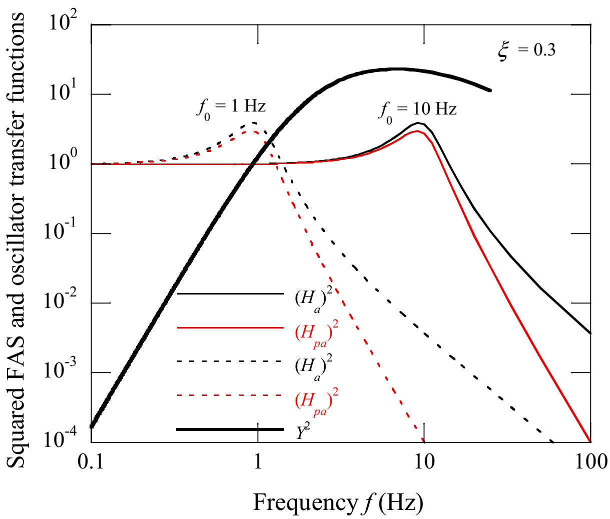

Fig. 8 Comparison of oscillator transfer functions for spectral and pseudospectral accelerations for different oscillator frequencies (1 and 10 Hz)

Content courtesy of Springer Nature, terms of use apply. Rights reserved.

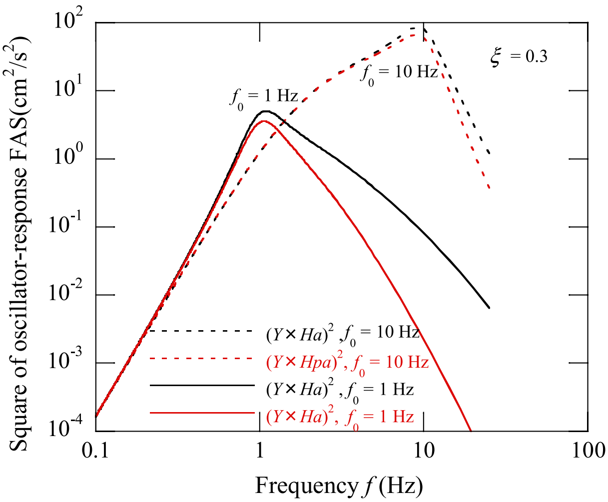

Fig. 9 Comparison of the square of the oscillator-response FAS for spectral and pseudospectral accelerations for different oscillator frequencies (1 and 10 Hz)

term. This conclusion can be easily verified by multiplying the FAS by a constant value; since a constant value is present in both the numerator and denominator of R_{rms}, they will cancel each other and will not affect R_{rms}. Therefore, the key factor affecting the seismological effects is the distribution of ground-motion FAS with frequency, i.e., the frequency content of the ground motions.

To investigate the variation of the frequency content of ground motions with the moment magnitude and site-to-source distance, the square values of the ground-motion FAS for two moment magnitudes and two site-to-source distances are compared in Fig. 10. It is noted that although the square values of FAS at all frequencies increase with increasing moment magnitudes, the increases in the low frequencies are more significant. This indicates that the low-frequency (or long-period) components of the earthquake ground motions increase relative to the high-frequency components with increasing moment magnitudes. Similarly,

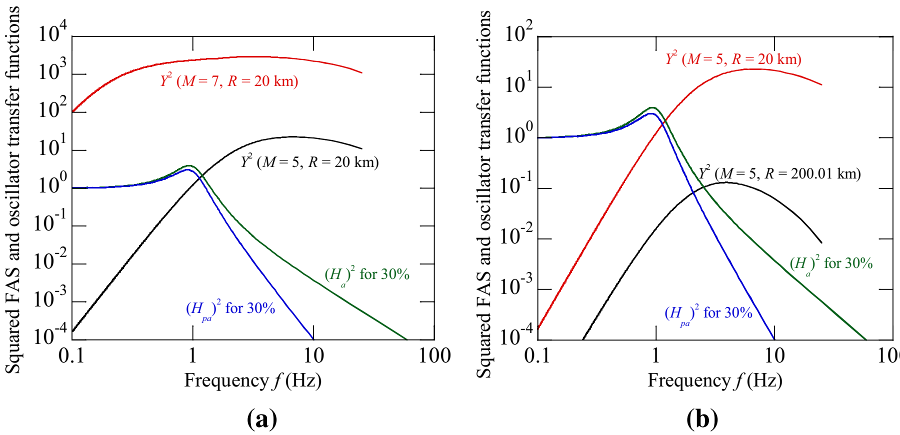

Fig. 10 Variation of the frequency content of ground-motion FAS with (**a**) moment magnitude and (**b**) site-to-source distance

Content courtesy of Springer Nature, terms of use apply. Rights reserved.

although the square values of FAS at all frequencies decrease with increasing site-to-source distances, the decreases at high frequencies are more significant. This means that the low-frequency components of the earthquake ground motions increase relative to the high-frequency components with increasing site-to-source distances. In addition, it is observed that the degree of variation of the frequency content of the ground motions with the site-to-source distances is smaller than that of the moment magnitude.

Based on the above properties of variation of the ground-motion frequency content, the *Sa*/*Spa* variation trends with the moment magnitude and site-to-source distance can be explained. It is important to once again emphasize that the spectral ratio *Sa*/*Spa* can be understood by investigating the differences between the two areas of the square of the oscillator-response FAS in Eq. (7), i.e., $\int_0^\infty \left|Y(\omega)H_a(\omega,\overline{\omega},\xi)\right|^2 d\omega$ and $\int_0^\infty \left|Y(\omega)H_{pa}(\omega,\overline{\omega},\xi)\right|^2 d\omega$. In addition, the square values of the oscillator-response FAS, i.e., $\left|Y(\omega)H_a(\omega,\overline{\omega},\xi)\right|^2$ and $\left|Y(\omega)H_{pa}(\omega,\overline{\omega},\xi)\right|^2$, are similar at the frequencies lower than the oscillator frequency f_0, but differ at the frequencies higher than f_0 (Fig. 9). For easier understanding, $\left|Y(\omega)H_a(\omega,\overline{\omega},\xi)\right|^2$ and $\left|Y(\omega)H_{pa}(\omega,\overline{\omega},\xi)\right|^2$ are further divided into two parts, respectively, as illustrated by Fig. 11. One part represents the area enclosed by the frequencies lower than the oscillator frequency f_0, where $\left|Y(\omega)H_a(\omega,\overline{\omega},\xi)\right|^2$ and $\left|Y(\omega)H_{pa}(\omega,\overline{\omega},\xi)\right|^2$ are similar, and is denoted as P_{I}. The other part represents the area enclosed by the frequencies higher than the oscillator frequency f_0, where $\left|Y(\omega)H_a(\omega,\overline{\omega},\xi)\right|^2$ and $\left|Y(\omega)H_{pa}(\omega,\overline{\omega},\xi)\right|^2$ differ, and the second parts for *Sa* and *Spa* are denoted as $P_{\mathrm{II}a}$ and $P_{\mathrm{II}pa}$ ($P_{\mathrm{II}a} > P_{\mathrm{II}pa}$), respectively. Thus, the ratio of $\int_0^\infty \left|Y(\omega)H_a(\omega,\overline{\omega},\xi)\right|^2 d\omega$ and $\int_0^\infty \left|Y(\omega)H_{pa}(\omega,\overline{\omega},\xi)\right|^2 d\omega$ can be simplified as,

$$\frac{\int_0^\infty \left|Y(\omega)H_a(\omega,\overline{\omega},\xi)\right|^2 d\omega}{\int_0^\infty \left|Y(\omega)H_{pa}(\omega,\overline{\omega},\xi)\right|^2 d\omega} = \frac{P_{\mathrm{I}}+P_{\mathrm{II}a}}{P_{\mathrm{I}}+P_{\mathrm{II}pa}} \tag{12}$$

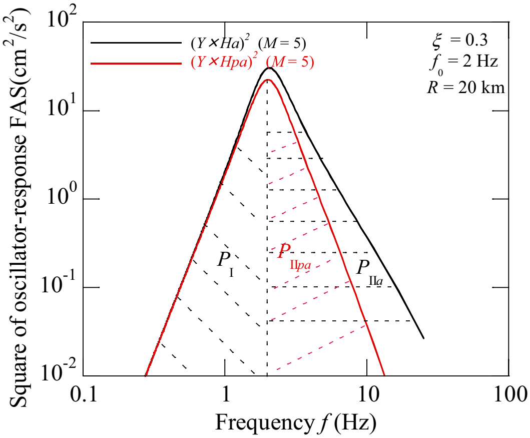

Fig. 11 Illustration of the areas of the square of the oscillator-response FAS enclosed by frequencies lower than the oscillator frequency f_0 (i.e., P_{I}) and higher than f_0 for *Sa* and *Spa*, (i.e., $P_{\mathrm{II}a}$ and $P_{\mathrm{II}pa}$)

Content courtesy of Springer Nature, terms of use apply. Rights reserved.

It is evident from Eq. (12) that when the similar part P_{I} increases relatively, the area ratio approaches unity, thus *Sa* approaches *Spa*; by contrast, when P_{I} decreases relatively, the area ratio increases and approaches $P_{\mathrm{II}a}/P_{\mathrm{II}pa}$, so that *Sa* deviates from *Spa*. Since the low-frequency components of the ground motions increase relatively with increasing moment magnitudes and site-to-source distances (Fig. 10), the similar part P_{I} lower than the oscillator frequency f_0 will increase relative to the part at frequencies higher than f_0, as shown in Fig. 12. Therefore, the area ratio expressed by Eq. (12) approaches unity with increasing moment magnitudes and site-to-source distances. This explains why *Sa* approaches *Spa* with increasing moment magnitudes and site-to-source distances, as shown in Figs. 3 and 4.

5 Practical *Sa*/*Spa* formulation

5.1 Formulation construction

A simple *Sa*/*Spa* formulation is constructed in this section considering the seismological effects for practical use in seismic design. To this end, a large number of function forms are trialed to fit the *Sa*/*Spa* results in Sect. 3. Finally, considering a balance between accuracy and simplicity, a simple *Sa*/*Spa* formulation is proposed that is given by

$$\frac{Sa}{Spa} = 1 + \left(0.14\xi^{1.54}\zeta^{-0.57}\right)T_0^{\xi^{-0.2}/\left(5\sqrt{\zeta}+1\right)} \tag{13}$$

where ζ is a parameter reflecting the seismological effects on *Sa*/*Spa*, as described in detail below. This equation satisfies the boundary condition that when the oscillator period T_0 and damping ratio ξ decrease to zero, *Sa*/*Spa* equals unity. Equation (13) also captures the *Sa*/*Spa* trends with variations in the oscillator period and damping ratio observed in Figs. 2, 3, 4 and previous studies using real seismic records (Sadek et al. 2000; Papagiannopoulos et al. 2013).

Because the seismological parameters (particularly the moment magnitude *M*) can significantly influence *Sa*/*Spa*, as observed above, Eq. (13) incorporates the seismological

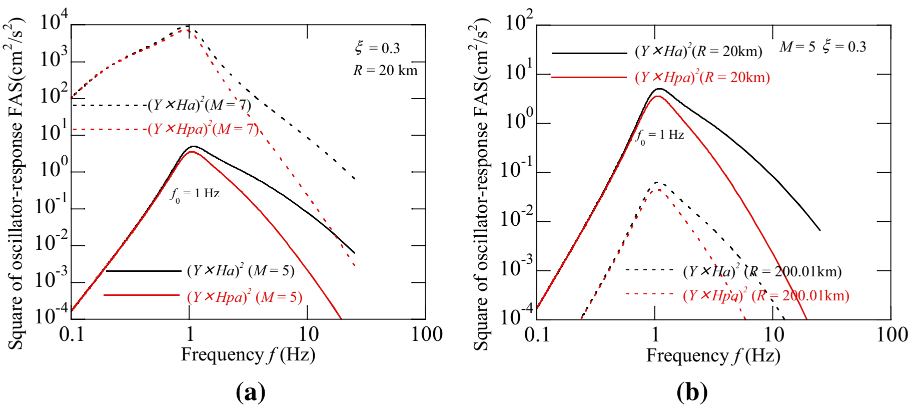

Fig. 12 Variations of the square of the oscillator-response FAS for spectral and pseudospectral accelerations with (**a**) moment magnitude and (**b**) site-to-source distance

Content courtesy of Springer Nature, terms of use apply. Rights reserved.

effects. In principle, the seismological parameters such as the moment magnitude M and site-to-source distance R should be explicitly included in the *Sa*/*Spa* formulation. However, since seismic design codes, e.g., ASCE/SEI 7–16 (2016) and Eurocode 8 (2004), typically only define *Spa* as the seismic load without providing these parameters, a formulation including such parameters is unrealistic for practical seismic design. Section 4 indicates that the seismological effects on *Sa*/*Spa* are governed by the frequency content of the ground motion; therefore, a parameter related to the frequency content can be adopted to reflect the seismological effects. Various frequency-content parameters have been defined based on the FAS and response spectra of ground motions (Craifaleanu 2011). Because only *Spa* is typically specified in seismic codes, four parameters available from *Spa* that were introduced by Craifaleanu (2011)—specifically, the predominant period T_{gSV}, modified spectral characteristic period T^*_{mean}, modified central period T^*_{cen}, and modified shape factor q^*—were tested. It is found that (not shown here), although the four parameters are closely related to moment magnitude and site-to-source distance, when they are applied to derive the *Sa*/*Spa* formulation, the estimated results are not sufficiently stable. Therefore, another frequency-content parameter ζ that can be obtained from *Spa* is adopted to reflect the seismological effects. This parameter is given by

$$\zeta = \frac{Spa(6\mathrm{s})}{\mathrm{PGA}} \tag{14}$$

where, *Spa* (6 s) and PGA are the values of *Spa* at 6 s and peak ground acceleration (i.e., *Spa* at 0 s) for a 5% damping ratio, respectively. It can be seen from Eq. (14) that ζ can be easily obtained from the *Spa* specified in seismic codes.

It can be easily known from Eq. (14) that ζ is closely related to the frequency content of the ground motion. When the short-period components are dominant and the bandwidth is narrow, *Spa*(6 s) is small relative to PGA, thus ζ is small; when the long-period component increases and the bandwidth becomes large, *Spa*(6 s) increases relative to PGA, hence ζ will increase. Therefore, ζ typically increases with the long-period components and can simply reflect the frequency content of the ground motion. In fact, the use of the *Spa* values at periods 0 and 6 s was determined by trying numerous values at different periods; it is found that the use of these two values in Eq. (13) obtains the highest accuracy.

The *Sa*/*Spa* results calculated by Eq. (13) were compared to those in Sect. 3 and some representative comparisons are shown in Fig. 13. It is noted that Eq. (13) performs very well in the prediction of *Sa*/*Spa*, particularly in the period range $T_0 < 6$ s that is generally of interest in practical seismic design. The variation trends of the results calculated by Eq. (13) with the structural and seismological paraments are fully consistent with those for the results obtained by the time-series analysis. For most cases, although Eq. (13) slightly underestimates the *Sa*/*Spa* values compared to those obtained by time-series analysis, the average relative error for the cases in the period range $T_0 < 6$ s is limited to 10%.

5.2 Comparison with real seismic records

The *Sa*/*Spa* results produced by Eq. (13) were further compared to those of real seismic records. Since the seismological parameters in Eq. (1), e.g., stress drop and geometric attenuation, for CENA were used for the above analyses, for consistency, the seismic records for the verification were also selected from the regions of CENA. All seismic ground motions in the Pacific Earthquake Engineering Research Center (PEER) database from CENA were searched. A total of 367 seismic records (734 accelerograms)

Content courtesy of Springer Nature, terms of use apply. Rights reserved.

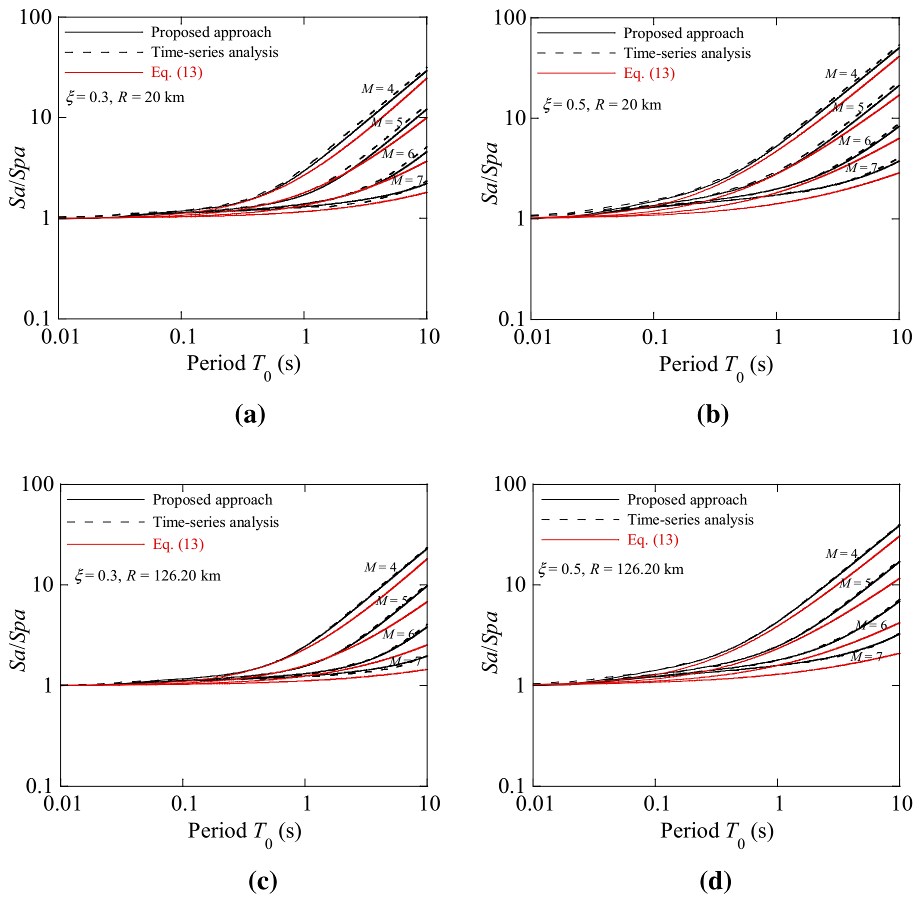

Fig. 13 Comparisons of *Sa*/*Spa* results from the proposed approach, time-series analysis, and Eq. (13) for the cases with oscillator damping ratio ξ and site-to-distance R of (**a**) $\xi = 0.3$, $R = 20$ km, (**b**) $\xi = 0.5$, $R = 20$ km, (**c**) $\xi = 0.3$, $R = 126.20$ km, and (**d**) $\xi = 0.5$, $R = 126.20$ km

with moment magnitude larger than 4.0 and rupture distance between 10 and 300 km were selected. Due to the lack of strong earthquakes in the regions of CENA, the largest moment magnitude of the selected records was limited to 5.85. The selected records were then classified into four groups considering a balance in the number of records, as shown in Fig. 14. It is found that the *Sa*/*Spa* results obtained by the proposed formulation are in good agreement with those of the real seismic records and show similar variation trends with the structural and seismological paraments, with the average relative error for the cases in the period range of $T_0 < 6$ s of approximately 5%.

In addition, the *Sa*/*Spa* results obtained in previous studies (Sadek et al. 2000; Song et al. 2007; Mentrasti 2008) are plotted in Fig. 14. It is clear from the figure that the proposed formulation shows better performance than existing methods that do not incorporate the seismological effects. The *Sa*/*Spa* results produced by the existing formulation basically correspond to the results with large moment magnitude.

Content courtesy of Springer Nature, terms of use apply. Rights reserved.

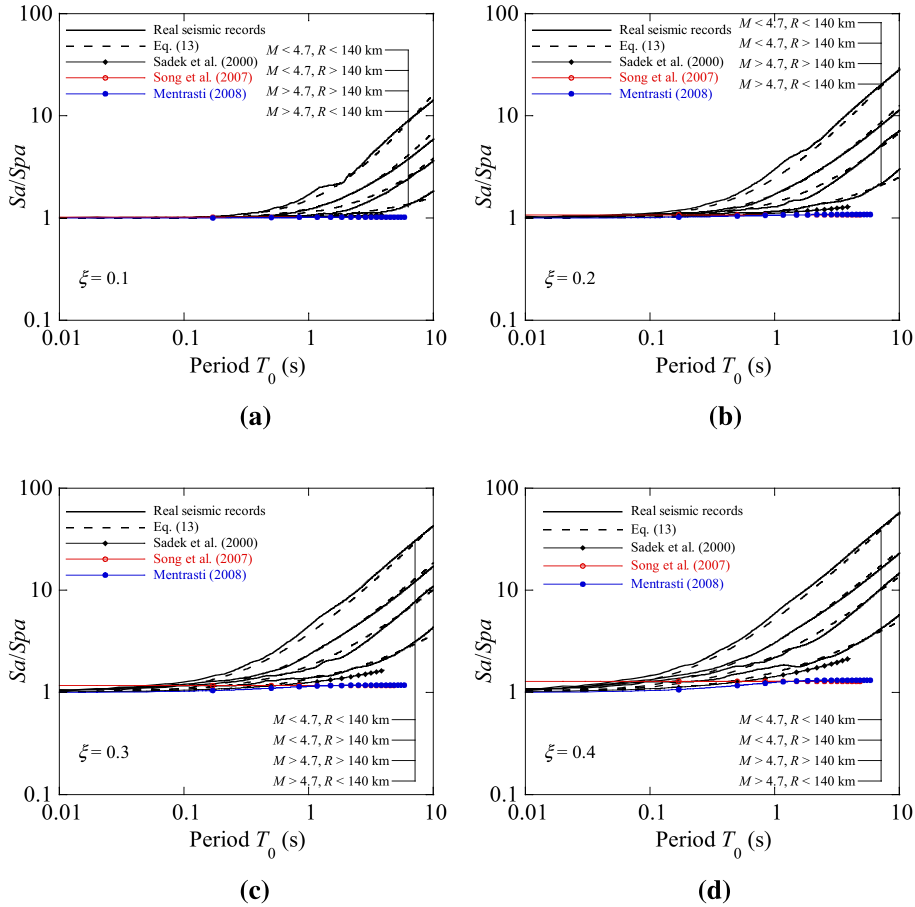

Fig. 14 Comparisons of *Sa*/*Spa* results from Eq. (13), real seismic records, and the formulations of Sadek et al. (2000), Song et al. (2007), and Mentrasti (2008) for the cases with oscillator damping ratio ξ of (**a**) $\xi = 0.1$, (**b**) $\xi = 0.2$, (**c**) $\xi = 0.3$, and (**d**) $\xi = 0.4$

5.3 Application of the proposed formulation

In this section, the proposed formulation (Eq. 13) is applied to calculate *Sa* from *Spa* for the estimation of the inertial forces. For this purpose, a 5%-damped *Spa* in the regions of CENA defined in ASCE/SEI 7–16 (2016) and the 5%-damped Type 2 *Spa* on type A ground specified in Eurocode 8 (2004) are used for analysis. The two 5%-damped *Spa* are normalized by PGA and adjusted considering an example structure with an equivalent damping ratio of 30% using the damping modification factors defined in ASCE/SEI 7–16 (2016) and Eurocode 8 (2004). Then, applying the proposed formulation, the *Sa*/*Spa* values for the damping ratio of 30% are calculated. Thus, *Sa* for the 30% damping ratio can be readily obtained by $Sa = Spa \times Sa/Spa$, with the results shown in Fig. 15. It can be found that for the design spectrum with relatively abundant long-period components (Fig. 15a), the difference between *Sa* and *Spa* is not large. However, the difference between *Sa* and *Spa* becomes significant for the design spectrum with relatively

Content courtesy of Springer Nature, terms of use apply. Rights reserved.

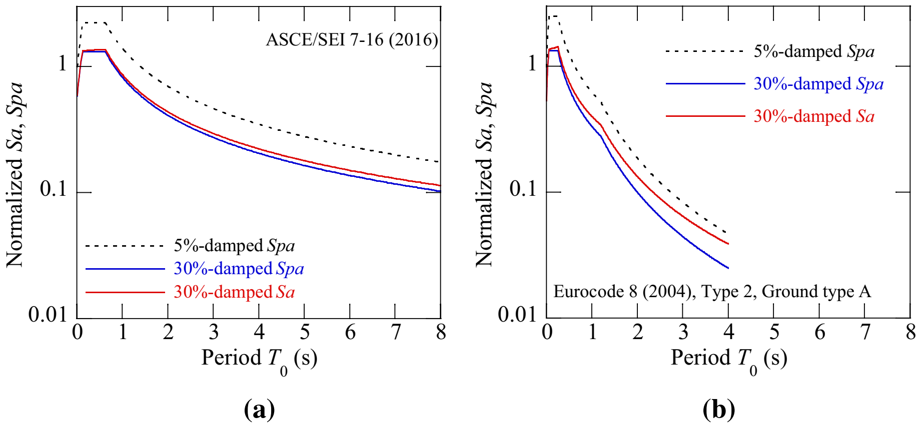

Fig. 15 Calculation of high-damping *Sa* from *Spa* using the proposed formulation for two design spectra in (**a**) ASCE/SEI 7–16 (2016), (**b**) Eurocode 8 (2004)

few long-period components (Fig. 15b). This variation trend of the *Sa*-*Spa* relationship with the frequency content is consistent with that described in Sect. 4. For the design spectrum in Eurocode 8 (2004), the values of the 30%-damped *Sa* at 4 s exceed those of the 30%-damped *Spa* by approximately 55%. This means that the use of *Spa* to approximate *Sa* will underestimate the inertial forces by approximately 55% for such cases. In addition, the *Sa*/*Spa* values for the two design spectra considering three damping levels are shown in Fig. 16. It can be seen from Fig. 16b that *Sa* is twice as large as *Spa* at approximately 4 s for a damping ratio of 50%. These results support that *Sa* may be significantly different from *Spa* for the design spectrum with few long-period components when the oscillator damping ratio is large and the oscillator period is long as is found for *Spa* in Eurocode 8 (2004).

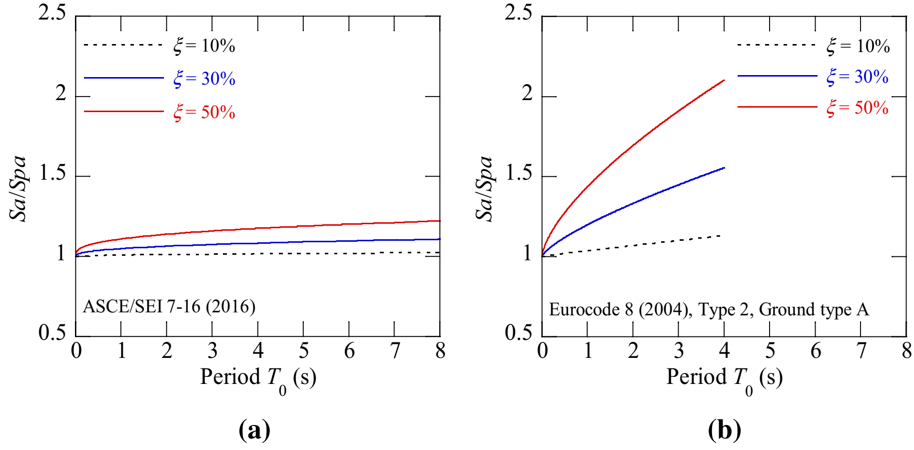

Fig. 16 Values of *Sa*/*Spa* for 10%, 30% and 50% damping ratios calculated by the proposed formulation for two design spectra in (**a**) ASCE/SEI 7–16 (2016), (**b**) Eurocode 8 (2004)

Content courtesy of Springer Nature, terms of use apply. Rights reserved.

6 Conclusions

In this study, an approach relating the spectral absolute acceleration *Sa* and pseudospectral acceleration *Spa* including seismological parameters was proposed based on random vibration theory. Using the proposed approach, the effects of the moment magnitude and site-to-source distance on the relationship between the two spectra were systematically explored and theoretically explained. Finally, a practical formulation for estimating *Sa* from *Spa* considering the seismological effects was constructed. The main conclusions of this study are summarized as follows:

1. The comparisons of *Sa*/*Spa* results obtained by the proposed method and traditional time-series analyses show that the proposed approach is valid.
2. The relationship between *Sa* and *Spa* is significantly affected by the moment magnitude and slightly affected by the site-to-source distance. Although the spectral absolute acceleration *Sa* becomes larger than the pseudospectral acceleration *Spa* as the structural period and damping ratio increases, this increase becomes smaller with increasing moment magnitude and source-to-site distance.
3. The key factor governing the seismological effects on the *Sa*-*Spa* relationship is the frequency content of the ground motions. The *Sa*/*Spa* variation trends with the moment magnitude and site-to-source distance can be reasonably explained by the variation of the frequency content with the seismological parameters.
4. The proposed simple *Sa*/*Spa* formulation is demonstrated to perform very well for a wide range of structural periods utilized in practical seismic design through a comparison to the results of real seismic records.

Acknowledgements This study was partially supported by the National Natural Science Foundation of China (Grant No. 51738001); the support is gratefully acknowledged. The authors are also grateful to Baojian Hang for help with the illustration of the figures in this paper. The authors also wish to thank Associate Editor John Douglas, Prof. David M. Boore, Prof. Sanjay Singh Bora as well as an anonymous reviewer for the constructive feedback and comments which led to significant improvements in the article.

Authors' contributions Haizhong Zhang: conceptualization, methodology, writing-original draft preparation, investigation. Yan-Gang Zhao: data curation, visualization, supervision, writing-reviewing and editing.

Funding The research leading to these results received funding from the National Natural Science Foundation of China (Grant No. 51738001).

Data availability All data generated or analyzed during this study are included in this published article.

Code availability Available upon request.

Declarations

Conflict of interest The authors have no conflicts of interest to declare that are relevant to the content of this article.

References

Akkar S, Sandıkkaya MA, Ay BÖ (2014) Compatible ground-motion prediction equations for damping scaling factors and vertical-to-horizontal spectral amplitude ratios for the broader Europe region. Bull Earthq Eng 12:517–547

Content courtesy of Springer Nature, terms of use apply. Rights reserved.

Alamilla JL, Rodriguez JA, Vai R (2020) Unification of different approaches to probabilistic seismic hazard analysis. Bull Seismol Soc Am 110(6):2816–2827

Architectural Institute of Japan (AIJ), (2001) Recommendations for design of building foundations, AIJ, Tokyo. (In Japanese)

ASCE/SEI 7-16 (2016) Minimum design loads for buildings and other structures. American Society of Civil Engineers, Reston

Atkinson GM, Boore DM (2014) The attenuation of Fourier amplitudes for rock sites in eastern north America. Bull Seismol Soc Am 104(1):513–528

Boore DM (1983) Stochastic simulation of high-frequency ground motions based on seismological models of the radiated spectra. Bull Seismol Soc Am 73(6A):1865–1894

Boore DM (2003) Simulation of ground motion using the stochastic method. Pure Appl Geophys 160:635–676

Boore DM, Joyner WB (1984) A note on the use of random vibration theory to predict peak amplitudes of transient signals. Bull Seismol Soc Am 74(5):2035–2039

Boore DM, Thompson EM (2012) Empirical improvements for estimating earthquake response spectra with random-vibration theory. Bull Seismol Soc Am 102(2):761–772

Boore DM, Thompson EM (2014) Path durations for use in the stochastic-method simulation of ground motions. Bull Seismol Soc Am 104(5):2541–2552

Boore DM, Thompson EM (2015) Revisions to some parameters used in stochastic-method simulations of ground motion. Bull Seismol Soc Am 105(2A):1029–1041

Boore DM (2001) Comparison of AA, PA and RV, PV for $M_L = 4.5$ and 7.1 earthquakes. http://daveboore.com/daves_notes/aa_pa_rv_pv_2.pdf.

Boore DM (2005) SMSIM: Fortran programs for simulating ground motions from earthquakes: version 2.3, A Revision of OFR 96–80-A, U.S. Geol Surv Dep Interior

Boore DM (2015) Point-source stochastic-method simulations of ground motions for the PEER NGA-East project, in NGA-East: median ground-motion models for the central and Eastern North America Region, Chapter 2, PEER Report 2015/04, Pacific Earthquake Engineering Research Center, 11–49

Cartwright DE and Longuet-Higgins MS (1956) The statistical distribution of the maxima of a random function. Proceedings of the Royal Society of London Series A, Mathematical and Physical Sciences 237:212–232

Chang KC, Lin YY (2004) Seismic response of full-scale structure with added viscoelastic dampers. J Struct Eng 130(4):600–608

Chopra AK (2007) Elastic response spectrum: a historical note. Earthq Eng Struct Dynam 36(1):3–12

Constantinou MC, Soong TT, Dargush GF (1998) Passive energy dissipation systems for structural design and retrofit, monograph series, MCEER, Buffalo, New York

Craifaleanu IG (2011) Investigation of the frequency content of ground motions recorded during strong Vrancea earthquakes, based on deterministic and stochastic indices. Eighth International Conference on Structural Dynamics, EURODYN, Leuven, Belgium, July 4–6, paper no. MS16–832 (on CD/ROM)

Davenport AG (1964) Note on the distribution of the largest value of a random function with application to gust loading. Proc Inst Civ Eng 28(2):187–196

Douglas J (2021) Ground motion prediction equations 1964–2021. http://www.gmpe.org.uk

Eurocode 8 (2004) Design of structures for earthquake resistance - part 1: general rules, seismic actions and rules for buildings. Brussels: European Committee for Standardization

Jenschke VA, Clough RW, and Penzien J (1964) Analysis of earth motion accelerograms. Report No. SESM 64–1, University of California, Berkeley, CA

Jenschke VA, Clough RW, and Penzien J (1965) Characteristics of strong ground motions. Proceedings of the Third World Conference on Earthquake Engineering III, New Zealand, 125–142

Kottke AR, Rathje EM (2013) Comparison of time series and random-vibration theory site-response methods. Bull Seismol Soc Am 103(3):2111–2127

Lin YY, Chang KC (2003) Study on damping reduction factor for buildings under earthquake ground motion. J Struct Eng 129(2):206–214

Liu L, Pezeshk S (1999) An Improvement on the estimation of pseudoresponse spectral velocity using RVT method. Bull Seismol Soc Am 89(5):1384–1389

Mentrasti L (2008) Estimate of spectral and pseudo-spectral acceleration proximity. Eng Struct 30(9):2338–2346

Naeim F and Kelly JM (1999) Design of seismic isolated structures. From theory to practice, John Wiley and Sons, New York

Newmark NM, Rosenblueth E (1971) Fundamentals of earthquake engineering. Prentice Hall, Englewood Cliffs, N.J.

Content courtesy of Springer Nature, terms of use apply. Rights reserved.

Nigam NC, Jennings PC (1969) Calculation of response spectra from strong-motion earthquake records. Bull Seismol Soc Am 59(2):909–922

Ohsaki Y (1996) Building vibration theory. Shokokusha Publishing Co., Ltd, Tokyo (**In Japanese**)

Papagiannopoulos GA, Hatzigeorgiou GD, Beskos DE (2013) Recovery of spectral absolute acceleration and spectral relative velocity from their pseudo-spectral counterparts. Earthq Struct 4(5):489–508

Pu W, Kasai K, Kabando EK, Huang B (2016) Evaluation of the damping modification factor for structures subjected to near-fault ground motions. Bull Earthq Eng 14:1519–1544

Rathje EM, Ozbey MC (2006) Site-specific validation of random vibration theory-based seismic site response analysis. J Geotech Geoenviron Eng 132(7):911–922

Sadek F, Mohraz B, Riley MA (2000) Linear static and dynamic procedures for structures with velocity–dependent dampers. J Struct Eng 126(8):887–895

Song J, Chu YL, Liang Z, Lee GC (2007) Estimation of peak relative velocity and peak absolute acceleration of linear SDOF systems. Earthq Eng Eng Vib 6(2):1–10

Vanmarcke EH (1975) On the distribution of the first-passage time for normal stationary random processes. J Appl Mech 42(1):215–220

Veletsos AS and Newmark NM (1964) Response spectra for single-degree-of freedom elastic and inelastic systems. Report No. RTD-TDR-63–3096, vol. III, Air Force Weapons Laboratory, Albuquerque, NM

Wada A, Huang YH, Iwata M (2000) Passive damping technology for buildings in Japan. Prog Struct Mat Eng 2(3):335–350

Wang X, Rathje EM (2016) Influence of peak factors on site amplification from random vibration theory based site-response analysis. Bull Seismol Soc Am 106(4):1733–1746

Wolff ED, Ipek C, Constantinou MC, Tapan M (2014) Effect of viscous damping devices on the response of seismically isolated structures. Earthq Eng Struct Dyn 44(2):185–198

Zhang HZ, Zhao YG (2020) Damping modification factor based on random vibration theory using a source-based ground-motion model. Soil Dyn Earthq Eng 136:1–11

Zhang D, Bai Y, Gao J (2016) Probe into several important concepts in Chinese current seismic response spectra. J Build Struct 37(4):110–118 (**In Chinese**)

Publisher's Note Springer Nature remains neutral with regard to jurisdictional claims in published maps and institutional affiliations.

Content courtesy of Springer Nature, terms of use apply. Rights reserved.

Terms and Conditions

Springer Nature journal content, brought to you courtesy of Springer Nature Customer Service Center GmbH ("Springer Nature").

Springer Nature supports a reasonable amount of sharing of research papers by authors, subscribers and authorised users ("Users"), for small-scale personal, non-commercial use provided that all copyright, trade and service marks and other proprietary notices are maintained. By accessing, sharing, receiving or otherwise using the Springer Nature journal content you agree to these terms of use ("Terms"). For these purposes, Springer Nature considers academic use (by researchers and students) to be non-commercial.

These Terms are supplementary and will apply in addition to any applicable website terms and conditions, a relevant site licence or a personal subscription. These Terms will prevail over any conflict or ambiguity with regards to the relevant terms, a site licence or a personal subscription (to the extent of the conflict or ambiguity only). For Creative Commons-licensed articles, the terms of the Creative Commons license used will apply.

We collect and use personal data to provide access to the Springer Nature journal content. We may also use these personal data internally within ResearchGate and Springer Nature and as agreed share it, in an anonymised way, for purposes of tracking, analysis and reporting. We will not otherwise disclose your personal data outside the ResearchGate or the Springer Nature group of companies unless we have your permission as detailed in the Privacy Policy.

While Users may use the Springer Nature journal content for small scale, personal non-commercial use, it is important to note that Users may not:

1. use such content for the purpose of providing other users with access on a regular or large scale basis or as a means to circumvent access control;
2. use such content where to do so would be considered a criminal or statutory offence in any jurisdiction, or gives rise to civil liability, or is otherwise unlawful;
3. falsely or misleadingly imply or suggest endorsement, approval , sponsorship, or association unless explicitly agreed to by Springer Nature in writing;
4. use bots or other automated methods to access the content or redirect messages
5. override any security feature or exclusionary protocol; or
6. share the content in order to create substitute for Springer Nature products or services or a systematic database of Springer Nature journal content.

In line with the restriction against commercial use, Springer Nature does not permit the creation of a product or service that creates revenue, royalties, rent or income from our content or its inclusion as part of a paid for service or for other commercial gain. Springer Nature journal content cannot be used for inter-library loans and librarians may not upload Springer Nature journal content on a large scale into their, or any other, institutional repository.

These terms of use are reviewed regularly and may be amended at any time. Springer Nature is not obligated to publish any information or content on this website and may remove it or features or functionality at our sole discretion, at any time with or without notice. Springer Nature may revoke this licence to you at any time and remove access to any copies of the Springer Nature journal content which have been saved.

To the fullest extent permitted by law, Springer Nature makes no warranties, representations or guarantees to Users, either express or implied with respect to the Springer nature journal content and all parties disclaim and waive any implied warranties or warranties imposed by law, including merchantability or fitness for any particular purpose.

Please note that these rights do not automatically extend to content, data or other material published by Springer Nature that may be licensed from third parties.

If you would like to use or distribute our Springer Nature journal content to a wider audience or on a regular basis or in any other manner not expressly permitted by these Terms, please contact Springer Nature at

onlineservice@springernature.com